Towards stable and highly active IrO_2 catalysts supported on doped tin oxides for the oxygen evolution reaction in acidic media

Sofia Delgado[1,2], *Paranjeet* Lakhtaria[1], *Eva* Sousa[1], *Tiago* Lagarteira[1], *K.A.* Friedrich[2] and *Adélio* Mendes[1*]

[1]Laboratory for Process Engineering, Environmental, Biotechnology and Energy (LEPABE), Faculty of Engineering of University of Porto, Rua Dr. Roberto Frias s/n, 4200-465 Porto, Portugal
[2]Institute of Engineering Thermodynamics, German Aerospace Center (DLR), Pfaffenwaldring 38-40, 70569 Stuttgart, Germany

Abstract. Iridium oxide is the preferred catalyst for water oxidation but it is required to maximize its utilization to deploy Proton Exchange Membrane Water Electrolyzers (PEMWEs) into the large-scale applications panorama. A promising pathway for dispersing this precious catalyst is on an electric conductive and stable support. However, there is a lack of understanding how the support-catalyst interactions affect the stability/activity of the electrocatalyst under anodic conditions. This work discloses a modified, easy-scalable, polyol synthesis protocol to produce a highly active and stable iridium-based catalyst, supported on metal-doped tin oxides. The loading of Ir was reduced 30 wt.% compared to the reference IrO_2, and dispersed on Sb-SnO_2 (IrOx/ATO), In-SnO_2 (IrOx/ITO) and SnO_2 supports. All synthesized electrocatalysts not only surpassed the OER-mass activity of a commercial catalyst (IrO_2) – reference – but also reached higher electrochemical active surface areas and enhanced stability under the OER conditions. The highest performance was achieved with Ir NPs supported on ITO (176 A/g_{Ir} *vs.* 15.5 A/g_{Ir} for the reference catalyst @ 1.51 V *vs.* RHE) and both IrOx/ITO and IrOx/SnO_2 catalysts demonstrated remarkable stability after cycling the electrode and performing long-term chronopotentiometry. ITO is, therefore, an auspicious support to serve Ir-based catalysts as it favors a good bargain between activity and stability, while drastically reducing the amount of noble metal.

Keywords. Proton Exchange Membrane Water Electrolyzer; Oxygen evolution reaction; Supports, Tin oxide

1 Introduction

Proton exchange membrane water electrolyzers (PEMWEs) exhibit excellent features for the production of green hydrogen, by mitigating the intermittency and fluctuation of renewable energy sources, and thus allowing the decarbonization of the electrical grids[1]. The oxygen evolution reaction (OER), considers the use of high noble metal loadings (*ca.* 2 to 4 $mg_{Ir}\cdot cm^{-2}$); even though the cost breakdown for the electrolyzer system addresses solely 5 % to the catalysts for small scale systems, considering the increasing energy demand and the needed widespread commercialization of PEM electrolysis, the catalysts still pose the major contributors for the prohibitive costs (1.9-2.3 k€/kW) [2–4]. For lowering the loading of such PGMs, the development of highly-structured catalysts that utilize PGM more effectively, the catalyst must display high mass activities, while being durable and possessing low volumetric packing density [5]. Overcoming these challenges will push PEM electrolysis into an economically feasible panorama to serve the large-scale production of green hydrogen.

By dispersing Ir catalysts onto high electrical conductive, large surface area (m^2/g) and highly corrosion resistant supports, there is a possibility to reduce the Ir-loading, while ensuring the maximum utilization of the noble metal to increase the OER mass activity [6]. These approaches are required to achieve the target for the reduction of today's Ir-specific power density in *ca.* 50-fold, down to *ca.* 0.01 g_{Ir}/kW while maintaining high efficiency (assuming electrolyzer efficiency of 70 % LHV – cell potential of *ca.*1.79 V) [7].

Non-noble metal oxides, specifically doped tin oxides (M-SnO_2) with hypovalent or hypervalent ions such as Sb, Nb, F, In, or Ta have been gaining momentum as they show great stability in strong acidic

* Corresponding author: mendes@fe.up.pt

media and delivering noteworthy electronic conductivities, surpassing 0.2 $S \cdot cm^{-1}$ [8–10]. As most metal oxides are semiconductors, doping them with such types of ions present the ultimate pre-requisite to allow an increase of electrical conductivities without compromising a path-free interconnected structure compatible with facile mass transport rates (water and oxygen).

The main objective of this work was to prepare highly active and stable IrO_2-based electrocatalysts via a facile modified polyol synthesis route and screen their activity and stability by carrying out different accelerated stress tests. In this regard, Ir- salt precursors were dispersed on different tin oxide-based nanoparticles, SnO2, SnO_2:Sb_2O_5 (-ITO) and SnO_2:In_2O_3(-ATO). A prepared 30 wt.% IrO_2 catalyst supported on SnO_2: In_2O_3 (1:1)/ 30IrO2/ITO allows to achieve a *ca.*11.5-fold larger OER activity and enhanced stability compared to a commercial benchmark catalyst, IrO_2. Moreover, remarkably *ca.* 3-fold larger BET surface area and electrochemical available surface areas could be achieved with IrOx/SnO_2 and IrOx/ITO, comparatively to IrO_2.

Extensive physico-chemical characterization acquired from TEM, TGA, ICP-OES, XPS, XRD and B.E.T physisorption analyses corroborate with the electrochemical measurements. To the best of the authors knowledge, the OER-mass activities herein reported of as-prepared catalysts (30IrO_2/ITO) are the highest at such operating conditions.

2 Experimental

2.1 Catalyst Preparation

Synthesis of electrocatalysts was carried out by adding 0.6 g of sodium hydroxide into 75 mL of ethane-1,2-diol (vwr) to produce a 0.2 M NaOH solution. This solution was sonicated and stirred for 3 hours. Antimony tin oxide (Sigma Aldrich, < 50 nm diameter), indium tin oxide (Sigma Aldrich, < 50 nm diameter) and tin oxide (Alfa Aesar, <30 nm) were used as received, added to the solution which was then sonicated for 45 minutes. The catalysts were then prepared via a chemical reduction of an IrO_2 salt precursor - $IrCl_3 \cdot xH_2O$ (Alfa Aesar) - in an ethane-1-2-diol solution kept at 175 °C for three hours. After the synthesis, 1 M nitric acid was added to adjust the pH of the solution to *ca.* 1 while stirring it for 4 h. The ratio of the salt precursor: support was maintained as 1:1 m/m. Later, the solution was filtrated and thoroughly washed using 1.5 L of ultra-pure water. The collected IrO_2 based nanoparticles were dried in an oven at 100 °C for 5 h.

2.2 Textural and physico-chemical characterization

Thermogravimetric analyses (TGA) were performed using a thermogravimetric analyser (TG 209 F1 iris, NETZSCH) under 30 cm^3 min^{-1} of airflow, and heating from room temperature to 1000 ºC at 2 ºC min^{-1}. *Ca.* 10 mg of catalyst powder was used in each analysis. The textural properties of each sample were evaluated by N_2 physisorption (-196 °C) in a Quantachrome Autosorb-1 Instruments device. The S_{BET} was obtained from the Brunauer-Emmett- Teller (BET) equation for a nitrogen partial pressure range of (P/P^0) from 0 to 1. The samples (*ca.* 50 mg) were outgassed in vacuum at 200 ºC overnight. Ir wt.% in each synthetized catalyst was confirmed with inductively coupled plasma – optical emission spectroscopy (ICP-OES; Thermo iCAP 7000). The solid samples of catalysts were completely dissolved in *aqua regia*, and, subsequently, diluted in deionized water prior to ICP-OES analyses, using a microwave digestor (Milestone, Start D). The bulk elemental composition of the IrO_2/M-SnO_2 catalysts was analyzed by energy dispersive X-ray spectroscopy (EDS) which was integrated in a Phenom ProX desktop scanning electron microscope (SEM).

2.3 Electrochemical characterization

2.3.1 OER activity and cyclic voltammograms - Cu_{UPD}

A catalyst suspension consisting of 5 mg of electrocatalyst, Nafion ionomer suspension (Quintech, 5 wt.%) and a mixture of ultrapure water (Millipore) and isopropanol (Merck) 1:4 was prepared via ultrasonication for 20 min at 20 kHz. Then, 20 µL of the prepared suspension containing 2.8 ± 0.1 μg_{Ir} was deposited and dried under rotation at 700 RPM on top of a 0.196 cm^2 Au working electrode tip. Electrochemical characterization was carried out in a rotating disk electrode (RDE) from PineResearch, equipped with a Gamry jacketed cell, a carbon rod and saturated Ag/AgCl in 3 M $KCl_{(aq)}$ which served as reference electrode. The bulk electrolyte 150 mL of 0.1 M $HClO_4$ solution was firstly saturated with Ar (mL/min) and a conditioning step took over consisting of 100 cycles from 0 V to 1.4 V vs RHE at 100 $mV \cdot s^{-1}$. Immediately after 3 cyclic voltammograms were retrieved at the same potential window at 20 mV/s.

An electrochemical impedance spectrum (EIS) was recorded to retrieve the ohmic resistance contribution from the electrolyte at 1 kHz with 10 mV of amplitude. Three linear sweep voltammograms were recorded at 2 mV s^{-1} to measure the OER specific activity at 1.51 V vs. RHE, and the ohmic resistance contribution was subtracted. The electrochemical performance of the prepared catalysts was compared with that of a commercially available IrO2 from Premetek, Co. To estimate the number of active sites available to process

the OER, a separate Cu_{upd} method was followed. The electrode was kept in a purged (Ar) 0.1 M H_2SO_4 electrolyte at 0.05 V *vs.* RHE for 10 minutes to reduce the reversible iridium oxide species formed throughout the synthesis. The electrode was cycled in the potential range from 0.2 V to 0.72 V *vs.* RHE at 20 mV for obtaining a first background CV. Afterwards, the electrode was reduced again for 15 min at 0.05 V. The first electrolyte was replaced by other containing 0.5 M H_2SO_4 and 5 mM of Cu_2SO_4 (Alfa Aesar). The electrode was cycled for 5 times (0.2 V to 0.72 V *vs.* RHE at 20 $mV \cdot s^{-1}$) to retrieve the Cu UPD voltammogram. Copper has a similar radius to that of metallic Iridium, 128 pm and 136 pm, respectively. By initially keeping the electrode at 0.05 V and then cycling it under these potentials, each Cu atom will adsorb/desorb on the surface of each iridium atom. By integrating the UPD (stripping) peak area it was possible to retrieve the amount of active Ir sites from each catalyst.

2.3.2 Stability Protocols

The first accelerated stress test (AST1) consisted of a controlled current electrolysis at 10 $mA \cdot cm^{-2}$ for 2 h under Ar saturated electrolyte, while keeping the electrode rotating at 1600 RPM [11] to avoid the accumulation of O_2 bubbles on top of the electrode. EIS, LSV and CV were again recorded to compare with initial performance. A second, separate AST, consisted of cycling the potential from 0.8 V – 1.0 V for 10 k cycles at the scan rate of 100 $mV \cdot s^{-1}$, while rotating the electrode at 200 RPM [11]; the latter serves as benchmark degradation protocol for heterogeneous catalysts to perform OER and therefore deeply understand the interaction between support and the catalyst.

3 Results and Discussion

3.1 Characterization of synthetised electrocatalysts

IrO_2 based catalysts supported on tin doped oxide nanoparticles were prepared following a polyol chemical reduction in alkaline media, as depicted in Fig. 1. The effective loading of Ir on each electrocatalyst was very similar for each prepared sample, *ca.* 30 ±2.3 wt.% as confirmed with ICP-OES. This proves that the synthesis was successful and the reaction conversion mostly complete.

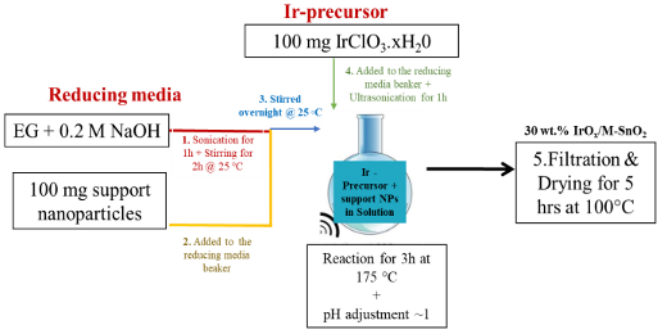

Fig. 1. Synthesis pathway to prepare IrO_2 supported on tin oxide-based nanoparticles via a polyol reduction in NaOH.

EDS analysis to the supports provided information regarding the weight concentration ratio of the dopants, Sn and In, Fig. 2; both represented 18 ± 0.06 wt.% of Sn and 47.6 ± 0.13 wt.% of the overall weight of the support, respectively.

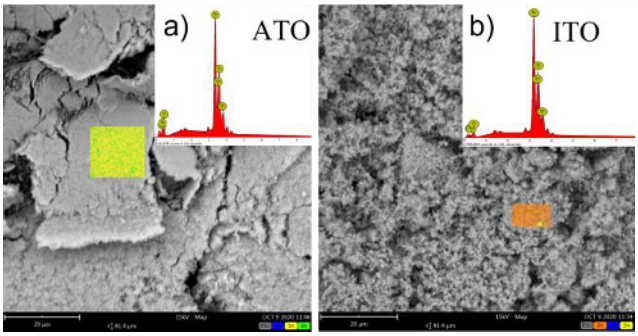

Fig. 2. EDS chemical mapping obtained for the supports a) ATO and b) ITO.

The thermal gravimetric decomposition curves of the synthesized catalysts and commercial IrO_2 demonstrate mainly two weight loss regions (as seen in Fig. 3). An immediate weight loss was detected for all the electrocatalysts except for IrO_2, from 90 °C to 220 °C and is attributed to the release of moisture from the 3D microstructure. As perceived from Table 1, 30IrO_2/ATO demonstrates the steepest weight loss (~8 %) due to the desorption of interstitial water and that could be attributed to its microstructure, as it is the one evidencing the largest pore volume and hence porosity; the latter is opposed to IrO_2 which appears to possess a more hydrophobic metallic nature and is, amongst all, the one owning the lowest pore volume and average pore diameter. From *ca.* 850 °C to 1000 °C, iridium tends to degrade from IrO_2 to IrO and the fact that Ir is dispersed on a tin oxide support enables to increase the thermal stability as the weight drop is less significant for all the prepared electrocatalysts comparatively, to non-supported commercial IrO_2 [12].

Overall, ITO containing catalyst depicted remarkable thermal stability up to 1000 °C with no significant weight variation (loss of *ca.* 3 % of initial weight).

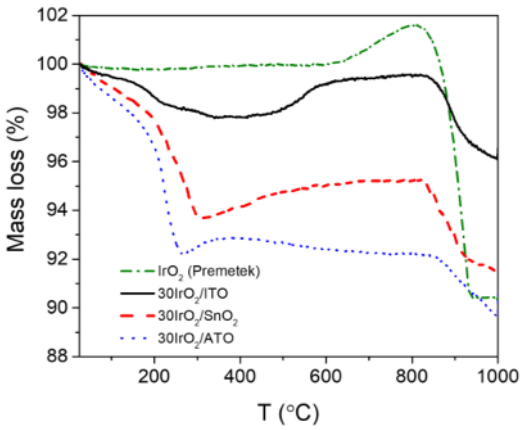

Fig. 3. TG curves for the prepared electrocatalysts from room temperature to 1000 °C under air flow – 200 mL·min^{-1}.

The activity of the synthesised electrocatalysts towards the OER, was derived from the average value of current at 1.51 V vs. RHE from three LSVs normalized by the mass of Ir in the working electrode. A scan rate of 2 mV·s^{-1} at 1600 RPM was used and the loading of the active metal, Ir, was kept similar throughout the experiments with the different electrocatalysts (10 μg_{Ir}·cm^{-2}). Fig. 4a) shows the OER polarisation curves and all the prepared electrocatalysts demonstrate an evident earlier onset happening at *ca.* 1.48 V vs. RHE comparatively to the benchmark catalyst. In fact, solely after an overpotential of nearly 390 mV does IrO_2 initiate the OER.

The kinetic mechanisms are facilitated for the remaining catalysts as a much lower overpotential is required to deploy the reaction, in detail: 30IrO_2/ITO (η=240 mV) < 30IrO_2/SnO_2 (255 mV) < 30IrO_2/ATO (η *ca.* 270 mV). Moreover, considerably higher limiting current densities can be achieved at such lower overpotentials, specially for ITO and SnO_2 supported IrO_2 catalysts, both reaching *ca.* 55 mA·cm^{-2} @ 1.58 V vs. RHE.

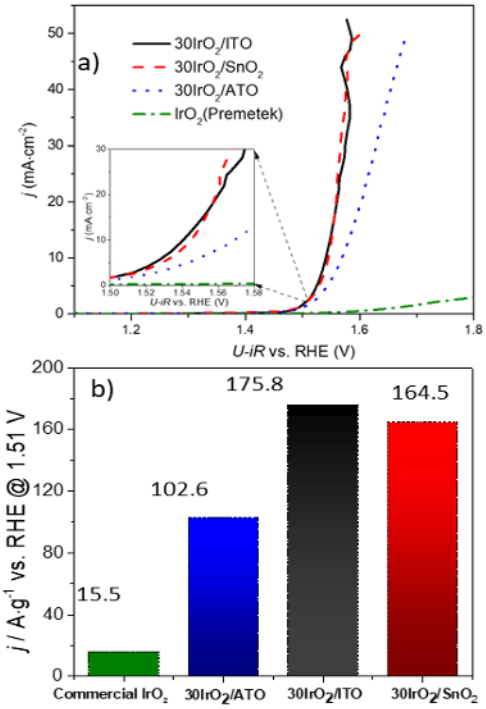

Fig. 4. a) OER polarisation curves for the studied catalysts retrieved at 2mV/s in Ar- saturated electrolyte 0.1 M $HClO_4$ at 1600 RPM and b) OER-mass specific activities retrieved at 1.51 V vs RHE normalized per the equal mass of Ir (2 ± 0.2 μg_{Ir}) in the Au tip (0.196 cm^2) for each catalyst.

The OER-mass specific activity for each catalyst is described in detail in Fig. 4b). A 11.5-fold higher MA could be attained with the prepared catalyst consisting of 30 wt.% of Ir(Ox) supported on ITO (where the dopant In represents *ca.* 33.4 % of the total electrocatalyst weight) vs the commercially available catalyst. Therefore, this electrocatalyst together with the dopant free SnO_2 IrO_2-based catalyst emerge as some of the highest and most promising OER supported catalysts ever reported at low Ir loadings at such operating conditions (175.8 and 164.8 mA/g @1.51 V for 10µg·cm^{-2} at 1600 RPM). Fig. 5 shows the CV curves for the prepared electrocatalysts and the commercial IrO_2 at 20 mV·s^{-1} in 0.1 M $HClO_4$.

Undoubtedly, the type of support deeply influences the reversibility of the system, as the redox couples shift slightly in the potential window to more reducing or oxidative potentials. However, the most symmetric CV and most likely electrochemically reversible electrocatalyst appears to be 30IrO_2/ITO since the peak-to-peak potential difference is small (certainly below < 57 mV at 25 °C) and the ratio between the anodic and cathodic peak/ forward-reverse scan peak current ratios reaches the ideality ($i_{pa}/i_{pc} \approx 1$) [13,14]; ITO-based electrocatalyst is the one exhibiting the more evident and symmetric set of redox peaks from 0.85 V to 0.95 V vs RHE attributed to the Ir^{3+}/Ir^{4+} redox reaction whilst the defined peaks emerging at 1.2 V to 1.35 V refer to the oxidation of Ir from Ir^{+4} to Ir^{5+} (forward scan) [15]. Several works report iridium valence states of $n \geq +4$ as

OER active but unstable, as dissolution mechanisms are generally triggered by the appearance of higher oxidation states.

Thereupon, among the synthesized catalysts, it is predictable that the catalyst $30IrO_2$/ITO may be more stable although not necessarily more active, at higher potentials comparatively to SnO_2 or ATO-supported catalysts [16]. All the catalysts have originated a hydrous Ir oxide (IrOx) specie. as if there was any Ir metallic character. The respective set of peaks would have appeared at low potentials 0.05 V < *U*< 0.35 V vs RHE.

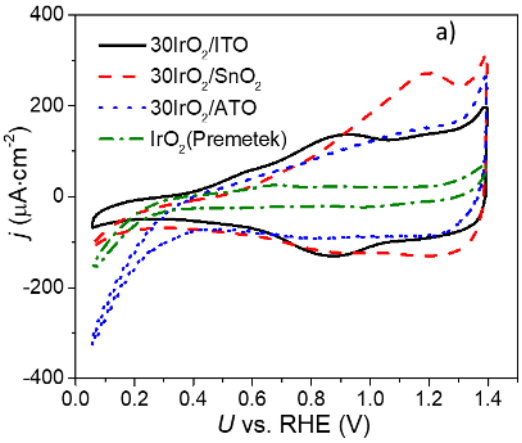

Fig. 5. Cyclic voltammograms of the synthetized electrocatalysts under Ar- saturated 0.1 M $HClO_4$ electrolyte at 20 $mV \cdot s^{-1}$ potential scan rates.

Cu_{UPD} was used as *in-situ* method to derive the active surface area of each catalyst. Table 1 presents the results for the attained charge related to the adsorption of Cu^{2+} ions on each iridium atom. Both SnO_2 and ITO display the greatest adsorbed charge, which is proportional to a larger number of effective active crystal planes from the supported IrO_2 (*ca.* 3-fold and 2-fold higher electrochemical total charge for $30IrO_2/SnO_2$ and $30IrO_2$/ITO, respectively and relatively to the commercial IrO_2). These results corroborate BET results and, although the OER-MA is slightly higher for $30IrO_2$/ITO while the surface areas are marginally superior for $30IrO_2/SnO_2$, it is important to address the morphology of the catalysts as it may be that the crystallinity and number of most active Ir facets is superior for the former ($30IrO_2$/ITO).

Besides, IrO_2 nanoparticles dispersed on ITO and SnO_2 revealed an average particle size of 2.4 nm and 2.9 nm compared to *ca.* 6.3 nm for those supported on ATO; all the former also approached a more acicular/round shape utterly distinct from the ordered IrO_2 nanoclusters, which present an average diagonal length of about 21.8 nm; typically, the electrochemical active area decreases with increasing average particle size.

Table 1. B.E.T estimated surface area, pore volume, average pore diameter and effective charge associated to Cu_{UPD}.

	IrO_2	**IrO_2/ATO**	**IrO_2/ITO**	**IrO_2/SnO_2**
B.E.T surface area ($m^2 \cdot g^{-1}$)	96.4	135.4	150.1	152.0
Pore Volume ($cm^3 \cdot g^{-1}$)	0.140	0.245	0.192	0.158
Avg. Pore Diameter (nm)	2.96	3.11	3.30	3.12
Cu_{UPD} adsorbed charge ($C \cdot s^{-1}$)	36.1	57.4	73.5	100.8

3.2 Stability tests

Concerning the first degradation protocol and the figure of merit for the OER activity Fig. 6a), which correlates the overpotential required to reach 10 $mA \cdot cm^{-2}$ after a specific period (2 h), it is possible to rapidly assess the stability of the stressed catalysts. The centred dashed line represents the potential dependant ideal catalyst response.

The overpotential of $30IrO_2$/ITO throughout the chronopotentiometry remained practically unchanged and therefore the deviation from the ideal behaviour is small, comparatively to the remaining electrocatalysts, as their final overpotential reached *ca.* 1 V *vs* RHE, including the commercial catalysts. By analysing the OER LSVs at Beginning of Life (BoL) and then at End of Life (EoL), Fig. 6b) and the limiting current density variation values from Table 2, it is quite noticeable the increment in mass transport limitations in all of them after the AST1. The commercial catalyst though, could barely endure the entire protocol, as there was no evident onset, and no current limited plateaux could be attained. The justification may rely in the fact that the mechanical integrity of the unsupported catalyst became compromised, perhaps due to the continuous entrapped bubbles of O_2 which may have triggered a dissolution mechanism or mechanical detachment from the working electrode into de bulk electrolyte - loss of 94 % of the initial limiting current density and 48 % of OER-MA loss with the long-term test. However, the presence of ITO, SnO_2:In_2O_3(1:1) as support appears to stabilize IrO_2 NPS thus contributing to the visible smallest drop in OER-activity (15 %).

But, overall, no evident conclusions may be associated with the fact that the use of dopants triggers dissolution mechanisms of Iridium, as described in recent works [17]; nonetheless the synthesis pathway is very distinct. On the other hand, OER activity and stability of the electrocatalyst $30IrO_2$/ITO is even superior compared to that of the undoped support (SnO_2); even so, the

$30IrO_2$/ATO, which contains a different dopant and lower ratio of Sb on the catalyst, delivers a lower performance comparatively to the undoped electrocatalyst. These results infer therefore, that the stability and OER-activity is highly dependent on the synthesis procedure and on the ratio between dopant and the active metal.

iR-corrected Tafel plots, Fig.6c) that display geometric normalized current on logarithmic scale, demonstrate a linear fit of the Butler-Volmer equation applied to potentials ranging from 1.45 V to 1.6 V vs RHE. Noticeable lower Tafel slopes at BoL could be acquired for the catalysts $30IrO_2$/ITO (41.4 mV·dec^{-1}) < $30IrO_2$/ATO (59.4 mV·dec^{-1}) < $30IrO_2/SnO_2$ (67.5 mV·dec^{-1}) < IrO_2 (93.1 mV·dec^{-1}), which corroborates to the 86 mV·dec^{-1}obtained in other works considering the same overpotentials [18].

After the AST, all the Tafel slopes increased at the same potential window indicating more complicated electron transfer processes possibly indicating the deterioration of the electrocatalysts; the causes for higher Tafel slopes may be attributed to increased mass transport resistance caused by the deterioration and rearrangement of the electrocatalysts' microstructure, loss of crystallinity, growth of Ir average particle size and consequently lower number of active sites or even detachment of active material from the WE surface.

Still, ITO supported IrO_2 catalyst shows the smallest increment in the Tafel slope (44.2 mV·dec^{-1}, *ca.* + 7 %), followed by $30IrO_2/SnO_2$ (83.3 mV·dec^{-1}= + 23.3 %), $30IrO_2$/ATO (81.9 mV·dec^{-1}= + 37.9 %). The unsupported commercial IrO*2* catalyst clearly suffered excessive and evident undesirable modifications in the reaction mechanisms, as a much higher Tafel slope was originated (*ca.* 192 mV·dec^{-1} after the AST2). This indicates that consecutively higher overpotentials are needed as higher energy barrier is imposed to deploy OER. In this regard, ITO stands a reliable support to stabilize IrO_2 NPs for long term operation at steady current densities.

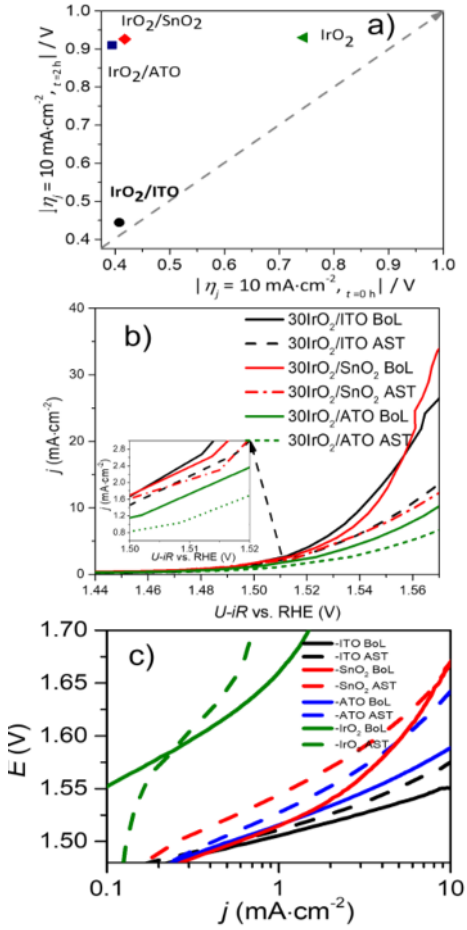

Fig. 6. a) Universal plot of merit for OER-MA activity and stability - the xx axis stands for the overpotential needed to achieve 10 mA/cm^{2}geo when t=0. The yy axis is the overpotential required to reach 10 mA·cm^{-2} time t=2 h; grey dashed diagonal represents the ideal output from a stable catalyst; b) OER polarisation curves at Beginning of Life (BoL) and after the AST1, End of Life (EoL) of the supported catalysts; c) corresponding Tafel plots for all the studied electrocatalysts (commercial IrO_2, $30IrO_2/SnO_2$, $30IrO_2$/ATO and $30IrO_2$/ITO) , before (bold) and after (dashed lines) the AST1 recorded at 2 mV·s^{-1} and 1600 RPM.

Table 2. Variation of current density values at plateaux and loss of OER mass activity after AST1.

AST1	**IrO_2**	**$30IrO_2$ /ATO**	**$30IrO_2$ /ITO**	**$30IrO_2$ /SnO_2**
Limiting current density at **BoL** (mA·cm^{-2})	10.8	21.7	52.4	49.7
Limiting current density at **EoL** (mA·cm^{-2})	0.66 (-94 %)	15.2 (-30 %)	22.3 (-57 %)	21.1 (-58 %)
OER-mass activity loss at EoL @ 1.51 V vs. RHE (%)	48	34	15	21

AST2 consisted of extensively cycling the potential for 10 k cycles from 0.8 V to 1.0 V vs RHE at 100 mV·s^{-1}. The potential window at which occurs the cycling stands for the conventional Ir(III)/Ir(IV) redox couple corresponding to the formation of the hydrous Ir – $IrO_x(OH)_y(H_2O)_z$.

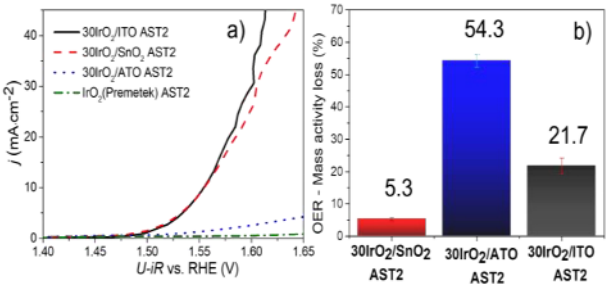

Fig. 7. a) OER polarisation curves EoL after the AST2; c) loss of OER mass activity, recorded at 1.51 V vs RHE at 2 mV·s^{-1} and 1600 RPM (10 µgIr·cm^{-2}).

Interestingly, the shape of CVs varied deeply, especially for the ATO supported and unsupported IrO_2 electrocatalysts, as an eminent loss of peaks could be perceived with a slightly shift to more oxidative potentials of the commercial catalyst. The later hints for the formation of unstable Ir oxidation states ($n \geq +4$), known to trigger degradation mechanisms and cause the loss of activity and inability of reaching a limiting current density plateaux, evident from Table 3 and Fig. 7a).

Table 3. Variation of current density values at plateaux and OER after AST2.

AST2	**IrO_2**	**30IrO_2/ ATO**	**30IrO_2/ ITO**	**30IrO_2/ SnO_2**
Limiting current density loss at **EoL** (%)	- 95	- 89	- 36	-51
OER-mass activity loss at EoL (%)	- 56	-54.3	-21.7	- 5.3

Once again, the catalyst 30IrO_2/ITO demonstrated superior stability and activity after the AST2, although the non-doped SnO_2 based catalyst demonstrated higher mass-activity – and a smaller performance drop after cycling (5.3% comparatively to BoL) - which might had been a direct cause of porosity increment throughout the catalyst´s microstructure, mainly micropores; in fact, higher MA may be associated to the a greater availability of active sites or reorientation of Ir facets to more active states, due to the intensive cycling on this region. However, 30IrO_2/SnO_2 demonstrate slightly higher mass transport limitations, comparatively to 30IrO_2/ITO (see Fig. 7b and limiting current density drop in Table 3).

4 Conclusion

A modified polyol chemical reduction synthesis route was effectively utilized to produce highly active and stable electrocatalysts consisting of 30 wt. % of noble Ir metal dispersed on ATO, ITO and SnO_2 nanoparticles.

The prepared catalysts not only demonstrated remarkably higher BET surface areas and larger effective electrochemical areas which in turn enabled these electrocatalysts to surpass the initial OER-activity of commercial IrO_2 in a maximum of *ca.*12-fold. Overall, dispersing Ir salt precursor onto these supports had a positive impact on the performance and stability of the prepared electrocatalysts. Important observations are:

- The stability of an electrocatalyst after either current controlling or potential cycling and the immediate EoL OER-activity is highly dependent on the synthesis procedure and on the ratio between dopant and the electrochemical active metal.
- The catalyst 30IrO_2/ITO with a dopant ratio of *ca.* 33 % on the overall electrocatalyst weight demonstrated the greatest initial OER-MA activity and showed comparable results in terms of activity and stability with the undoped counterpart, 30IrO_2/SnO_2, on delivering the best stability after both ASTs.
- AST2 caused the highest impact on loss of performance overall; the formation of less stable Iridium species (n >+4) was mainly triggered on unsupported IrO_2 and Sb doped (*ca.* 15 % dopant on total weight of catalyst) based catalysts.

In depth, investigations on the optimum ratio of In dopant/Iridium loading should be led following this synthesis method to tune this promising electrocatalysts and pave the way for the mass commercialization of PEMWEs for large scale applications.

Acknowledgment

This work was financially supported by the project UID/EQU/00511/2020 of the Laboratory for Process Engineering, Environment, Biotechnology and Energy – LEPABE - funded by national funds through FCT/MCTES(PIDDAC). Eva Sousa and Sofia Delgado are grateful to the Portuguese Foundation for Science and Technology (FCT) for the doctoral grants (references SFRH/BD/145412/2019 and SFRH/BD/144338/2019, respectively).

References

1. F. Smolinka, Tom.;Wiebe Nikolai.; Sterchele Philip.; Palzer, Andreas. ; Lehner, Franz.; Jansen, Malte.; Kiemel, Steffen.; Miehe, Robert.; Wahren, Sylvia.; Zimmermann, *Industrialisation of Water Electrolysis in Germany: Opportunities and Challenges for Sustainable Hydrogen for*

Transport, Electricity and Heat (Berlin, 2018)
2. U. Babic, M. Suermann, F. N. Büchi, L. Gubler, and T. J. Schmidt, J. Electrochem. Soc. **164**, F387 (2017)
3. M. Carmo, D. L. Fritz, J. Mergel, and D. Stolten, Int. J. Hydrogen Energy **38**, 4901 (2013)
4. K. E. Ayers, J. N. Renner, N. Danilovic, J. X. Wang, Y. Zhang, R. Maric, and H. Yu, Catal. Today **262**, 121 (2016)
5. C. Spöri, J. T. H. Kwan, A. Bonakdarpour, D. P. Wilkinson, and P. Strasser, Angew. Chemie - Int. Ed. **56**, 5994 (2017)
6. L. Wang, P. Lettenmeier, U. Golla-Schindler, P. Gazdzicki, N. A. Canas, T. Morawietz, R. Hiesgen, S. S. Hosseiny, A. S. Gago, and K. A. Friedrich, Phys. Chem. Chem. Phys. **18**, 4487 (2016)
7. M. Bernt, A. Siebel, and H. A. Gasteiger, J. Electrochem. Soc. **165**, F305 (2018)
8. H. Ohno, S. Nohara, K. Kakinuma, M. Uchida, and H. Uchida, (2018)
9. S. Geiger, O. Kasian, A. M. Mingers, K. J. J. Mayrhofer, and S. Cherevko, Sci. Rep. **7**, 1 (2017)
10. H.-S. Oh, H. N. Nong, and P. Strasser, Adv. Funct. Mater. **25**, 1074 (2015)
11. M. CC, J. S, P. JC, and J. TF, J. Am. Chem. Soc. **135**, 16977 (2013)
12. F. Karimi, B. A. Peppley, and A. Bazylak, ECS Trans. **69**, 87 (2015)
13. R. G. Compton and C. E. Banks, Underst. Voltammetry, 2nd Ed. 1 (2010)
14. A. J. Bard, J. Am. Chem. Soc. **129**, 242 (2007)
15. B. Zhang and D. S. Su, ChemCatChem **7**, 3639 (2015)
16. N. Danilovic, R. Subbaraman, K.-C. Chang, S. H. Chang, Y. J. Kang, J. Snyder, A. P. Paulikas, D. Strmcnik, Y.-T. Kim, D. Myers, V. R. Stamenkovic, and N. M. Markovic, J. Phys. Chem. Lett. **5**, 2474 (2014)
17. G. C. da Silva, S. I. Venturini, S. Zhang, M. Löffler, C. Scheu, K. J. J. Mayrhofer, E. A. Ticianelli, and S. Cherevko, ChemElectroChem **7**, 2330 (2020)
18. Z. Ma, Y. Zhang, S. Liu, W. Xu, L. Wu, Y. C. Hsieh, P. Liu, Y. Zhu, K. Sasaki, J. N. Renner, K. E. Ayers, R. R. Adzic, and J. X. Wang, J. Electroanal. Chem. **819**, 296 (2018)